Statistics on omega band properties and related geomagnetic variations

M. Vokhmyanin[1,2], S. Apatenkov[1], E. Gordeev[1], V. Andreeva[1], N. Partamies[3], K. Kauristie[4], and L. Juusola[4]

[1] Earth's Physics Department, St. Petersburg State University, St. Petersburg, Russia.

[2] Space Climate Research Group, Space Physics and Astronomy Research Unit, University of Oulu, Oulu, Finland.

[3] Department of Geophysics, University Centre in Svalbard, Longyearbyen, Norway.

[4] Finnish Meteorological Institute, Helsinki, Finland.

Corresponding author: Evgeny Gordeev (evgeny.i.gordeev@spbu.ru)

Key Points:

- Super-epoch analysis confirmed the typical ground magnetic variations for omega structure - bipolar pulse in By and short Bz decrease
- Omega structures produce 50-100% higher than averaged dB/dt during low and moderate geomagnetic activity
- Statistically confirmed that ground dB/dt value depends on omegas velocity and size.

Abstract

Using the list of the omega structures based on the The Magnetometers - Ionospheric Radars-Allsky Cameras Large Experiment (MIRACLE) network (Partamies et al. 2017), we obtained a number of important statistical characteristics describing the surface magnetic field. Based on 438 events, typical magnetic variation associated with the passage of the single omega were obtained. The typical variation, obtained using superposed epoch analysis, is associated with a local bending of the western electrojet and statistically confirms the distribution of equivalent ionospheric currents obtained in earlier observations of single omegas. It was found that during low and moderate geomagnetic activity, appearance of the omega structures in the dark morning MLT sector results in twice higher than average dB/dt on the ground surface. Also, the velocity, direction of movement , and area of omega structures were calculated. It is shown that faster and bigger omegas produce larger time derivatives of the ground magnetic field. Furthermore, we demonstrate that in the 03-08 MLT sector, superposed magnetic variations for the arbitrary events of very high time derivatives |dB/dt|>10nT/s, reveal magnetic signatures similar to omegas. Our findings, together with the results described in Apatenkov et al., 2020, emphasize the important role of omega structures in the formation of large geomagnetically induced currents.

1 Introduction

Auroral omega bands are specific auroral forms emerging as a set of quasi-periodic long-living undulations in the poleward side of diffuse auroral arc, which have typical scale size from several hundred to several thousand kilometers, life time up to 100 min and drift eastward with the speed of 0.4-2 km/s (Akasofu and Kimball, 1964; Henderson et al., 2001; Sergeev et al., 2003).

Based on the MIRACLE all-sky camera data from five identical Lapland stations, Partamies et al. (2017) have performed the largest statistical study of some omega band properties. Using semi-automated search methods, they detected 438 individual auroral omega structures in 1996-2007. Such representative statistics led to the following solid conclusions, complementing previous works. (1) Omega bands are typically observed in the morning sector towards the end of substorm expansion phase or during recovery phase (Akasofu 1974; Opgenoorth et al., 1994). It is worth to note, the omega bands tend to appear during higher than average substorm activity, characterized by averaged local electrojet index IL=-250 nT, which is almost twice as intense as the average IL level for all substorms detected in this region (Partamies et al., 2015). (2) An average altitude of peak emission within omega structures is 118 km. This gives an estimate of a few keV for the characteristic energy of precipitating electrons, which agrees with previous estimates (Amm et al., 2005; Wild et al., 2011). (3) Each individual omega was found to match with two-vortex equivalent Hall current structure associated with the pair of field-aligned currents where upward current corresponds to the bright part of omega undulation (Amm et al., 2005; Weygant et al., 2015).

The same set of omega structures from Partamies et al. (2017) was used by Andreeva et al. (2021) to statistically investigate the omegas' source location. The authors projected the omegas from the ionosphere to the magnetospheric equatorial plane, using the fresh empirical magnetic field model (Tsyganenko and Andreeva, 2016). Ionosphere-to-magnetosphere projection show that the omegas' source is located relatively close to Earth at radial distances of 6-13 R_E, supporting previous case study results (Liu et al.,2018; Wild et al., 2011; Weygand et al., 2015). Velocity estimates for omega projections revealed the radial earthward propagation of the omegas' source region at a typical speed of several tens of km/s, in addition to expected eastward propagation observed in the ionosphere (Opgenoorth et al., 1983; Sergeev et al., 2003).

In the present study, we will further extend the set of characteristic omega band properties using the same list of omegas from Partamies et al. (2017). Here, we will focus on the ground magnetic field perturbations, particularly dB/dt amplitudes, and their link to the kinematic characteristics such as size and drift velocity of omegas. The ground magnetic perturbations are of special interest for space weather applications since they cause geomagnetically induced currents (GIC) in long conducting systems – power grids, pipelines, railway grids (Pulkkinen et al., 2017).

Inductive coupling between dB/dt and electric field that drives GIC is not linear due to the finite Earth's conductivity, so a large but short dB/dt impulse does not necessary produce large GIC (Cagniard, 1953; Oyedokun et al., 2020). This nonlinearity in the dB/dt-GIC relationship is less pronounced for the lower frequency magnetic field variations with periods more than 1 minute, including Pi3/Ps6 range of pulsations (Heyns et al., 2021) inherent to omega bands (Saito, 1978; Gustafsson et al., 1981; Opgenoorth et al., 1983; Jorgensen et al. 1999; Viljanen et al., 2001). This gives confidence to use dB/dt as a proxy for GIC in the case of omega bands. In addition, it was shown in Apatenkov et al. (2020) that the largest GIC (>100 A) ever recorded in the Kola Peninsula power grid was caused by omega band activity, and the main inductive effect was linked to the spatial derivative associated with omega motion. Omega bands, being compact transient auroral phenomena, have localized but significant effect on the ground systems in high latitudes. In this paper, we study this effect for the first time on a statistical basis.

This paper is structured as follows. The all-sky camera data and the ground magnetic field data for the utilized set of omega cases are described in the next Section. Superposed ground magnetic variations are discussed in Section 3. In Section 4, we evaluate how the presence of omegas affects time derivatives of the geomagnetic field observed on the ground. In Section 5, we present the procedure to derive velocity, direction, and areas of the studied omega structures. In Section 6, we estimate the relation between maximum |dB/dt| and omega's velocity and area. Finally, in the discussion, we look on the typical magnetic variations corresponding to the extreme |dB/dt|>10 nT/s cases.

2 Instruments and data

Partamies et al. (2017) [hereinafter P17] provided a list of omega shape auroras which were observed with the All-sky cameras (ASC) at five MIRACLE network stations during 1996-2007. These stations are located in Fennoscandian Lapland at the auroral latitudes: Sodankylä (SOD, 63.92° N corrected geomagnetic latitude), Muonio (MUO, 64.72° N), Abisko (ABK, 65.30° N), Kilpisjärvi (KIL, 65.88° N) and Kevo (KEV, 66.32° N). P17 introduced a semi-automatic method to detect the omega shape auroras during the nighttime hours from September to April (when the Sun is more than 10 degrees below the horizon). In our statistical study we utilize the entire list of 438 omegas introduced in P17 paper.

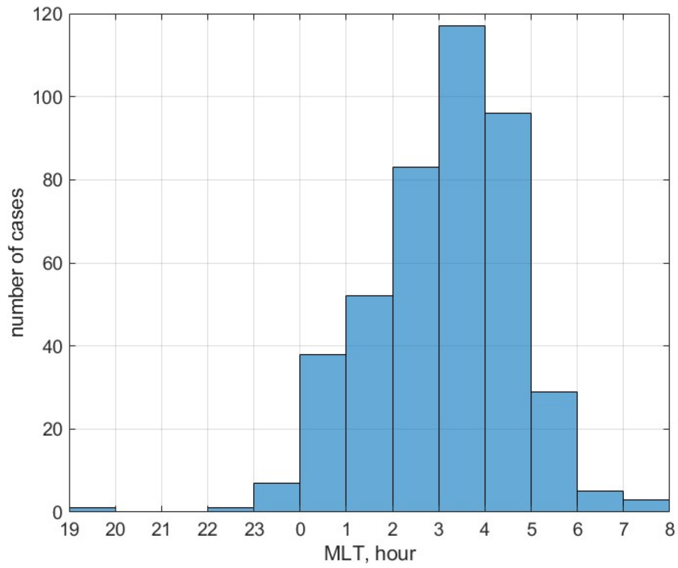

Figure 1. Magnetic local time distribution for the observed omega structures.

Figure 1 shows the distribution of omegas' magnetic local time (MLT) when most of the structure was well observed within the camera field of view. The selected cases occupy 23-08 MLT with 68% of the omegas observed within 02-05 MLT morning sector. Majority of the events (335) corresponds to an individual omega, i.e. the next omega appears after more than half an hour. The omegas are tracked within the ASC field of view from 4 to 15 minutes. Taking into account the average altitude of the observed in P17 omegas h=118 km, the size of the omegas is restricted to the area of a circle with diameter of about 600 km. Note that the horizontal scale size of omegas can be more than 1000 km (Tanaka et al. 2015).

Ground magnetic data were provided by the IMAGE network magnetometers (Tanskanen, 2009) at 10s time resolution at the same observatories with ASCs (20s resolution). The time derivatives and the variations of the geomagnetic field are investigated in three field components: horizontal X (northward), horizontal Y (eastward), and vertical Z (directed to the Earth's center).

In Figure 2, we include three examples of the ASC images captured at Sodankylä station at the following times 01:07:00 UT in 12 September 2002, 01:42:40 UT in 5 March 2001, and 01:38:20 in UT 02 October 2002. These examples show a large diversity of the shape, size, and brightness of omega structures. Below, we show the variations and time derivatives of the geomagnetic field components within ±10 minutes around the noted time. The amplitude of the perturbations significantly increases for brighter and bigger structures at Figure 2b and c. On the contrary, no pronounced magnetic effects are seen near the peak time corresponding to the faint omega in Figure 2a.

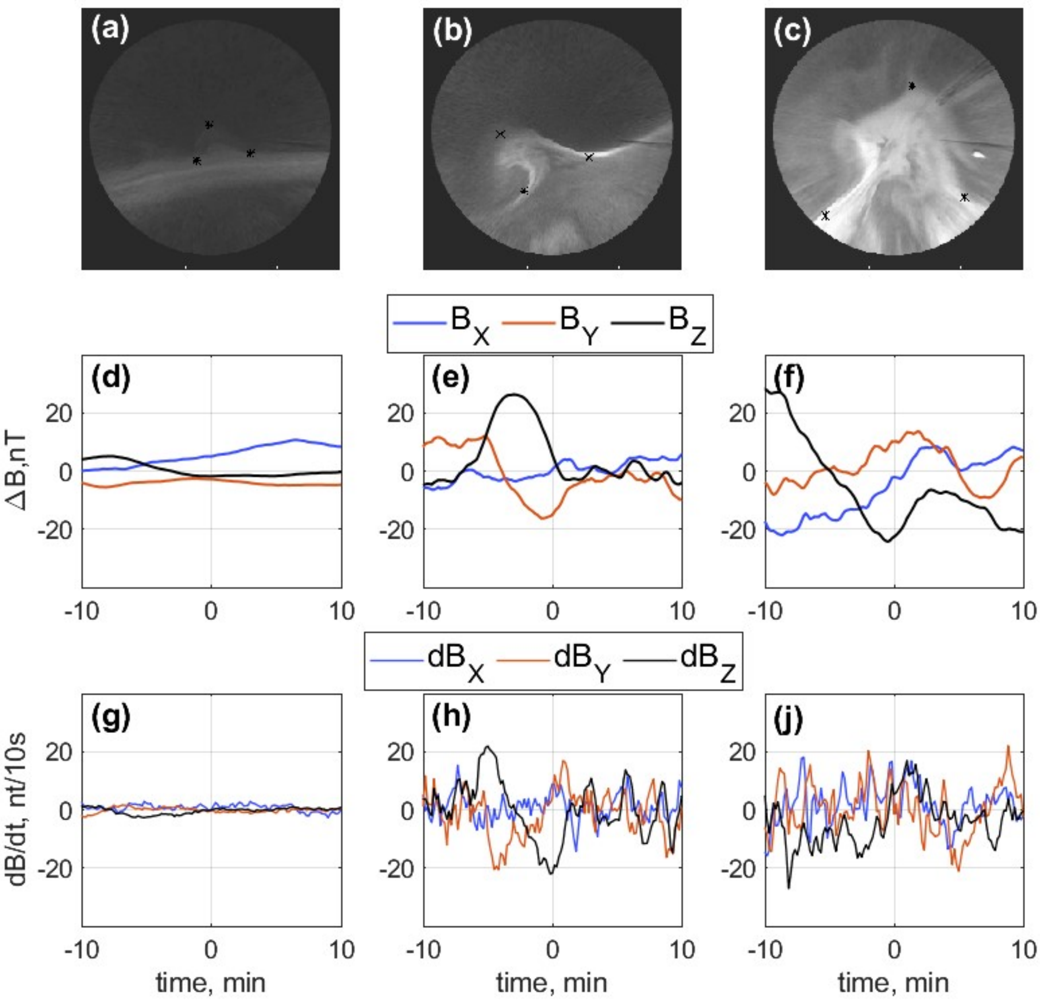

Figure 2. The examples of omega observations by the ASC at Sodankylä : a) 01:07:00 UT, 12 September 2002; b) 01:42:40 UT, 5 March 2001; c) 01:38:20 UT, 02 October 2002; below are the corresponding variations and time derivatives in X (blue), Y (red), and Z (black) components of the geomagnetic field within ±10 minutes of the time when the images were taken.

Figure 2 shows that not every individual omega has specific and clear magnetic signatures. The variations are different in shape and amplitude. Thus, a superposed epoch method is used to study the typical magnetic variations associated with an omega passage.

3 Results

3.1. Superposed geomagnetic variations

Using the geomagnetic data of the IMAGE network, we select one hour intervals which were centered with respect to the peak time (Partamies et al., 2017), which is the time when the most omega-like structure was observed within the ASC field of view. The magnetic data were recorded during different years and seasons so the baselines can differ dramatically. The averaged values were subtracted to be able to superpose and compare the magnetic variations. This is applied to every component. This is a very rough estimate of the background/baseline field. Nevertheless, this simple and fast procedure is suitable when studying the magnetic field variations rather than absolute values. Ps6 pulsations associated with omega bands (Saito, 1978) have periods 3-5 times shorter than one hour so the average value is expected to be close to the pulsations' "zero level".

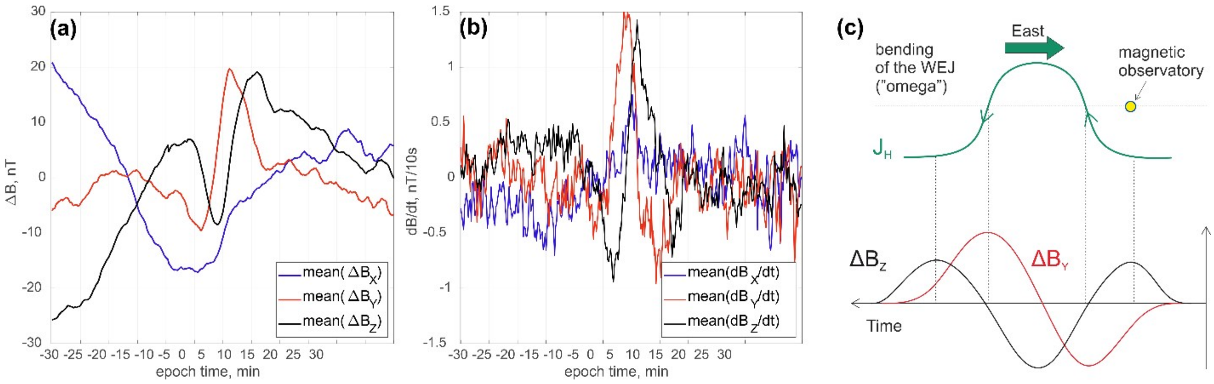

Figure 3. The examples of omega observations by the ASC at Sodankylä : a) 01:07:00 UT, 12 September 2002; b) 01:42:40 UT, 5 March 2001; c) 01:38:20 UT, 02 October 2002; below are the corresponding variations and time derivatives in X (blue), Y (red), and Z (black) components of the geomagnetic field within ±10 minutes of the time when the images were taken.

Figure 3a shows superposed variations of X (geographic North), Y (geographic East), and Z (downwards) geomagnetic field components for the entire set of 438 observed omegas. We found a surprising fact that so different individual magnetic recordings being summed up show the distinct variation attributed to the omega passage. Two time scales can be distinguished within these magnetic signatures: (1) short - ten minutes around the omega, ±5 minutes close to zero epoch time, and (2) long - about 30 minutes preceding to the omega.

The short time scale can be explained by eastward propagation of the ionospheric current structure typical for the omega. Opgenoorth et al. (1983) and Amm et al. (2005) show the intense current directed equatorward at the western part of the omega carried mainly by Hall current. Clear bipolar variations in Y and Z field components can be explained by the eastward propagation of this equatorward (southward for IMAGE) current. At the -5 min time moment (Figure 3a) the current is on the west side from the station, at the +5 min time moment the current propagates eastward and appears on the right side. We show this propagation schematically in Figure 3c. Note that time goes to the left on the sketch, i.e. opposite to that in the observations.

The longer variation has no such straightforward and expected explanation, we interpret it as an equatorward expansion of the westward electrojet (WEJ). Decrease of Bx is caused by the approaching westward current and/or its intensity growth. The growth of Bz and its sign change from negative to positive denotes the equatorward propagating WEJ: at -30 min time moment the current was poleward from the station, at -10 min the current was located overhead or even passed further equatorward. Note that the effect in Figure 3a is only a qualitative estimate. The amplitude of the effect is about 30 nT but might be significantly higher (see Figure 4 for example) for individual cases - the standard deviation of the field values observed within the ±5 min time is about 50 to 60 nT.

In Figure 3b, the average time derivatives (dB/dt is expressed in nT per 10 seconds) reveal the presence of the omega effect even more clearly. Distinctive dB/dt signature stands out from the background noise within the ±5 minutes of zero epoch time. Result in Figure 3b was obtained without any manipulations with the data, like background field subtraction, and should be considered as a more reliable evidence of the magnetic effect of the omegas. The mean amplitude of superposed time derivatives is about 1.0 to 1.5 nT/10 s, while the standard deviation of the observed values is about 4 nT/10 s. The most probable time to see the highest dB/dt is when the omega moves right over the observation site within ±5 minutes of zero epoch time. Overall, omegas increase the probability of high dB/dt observation which is discussed in more detail in the next section.

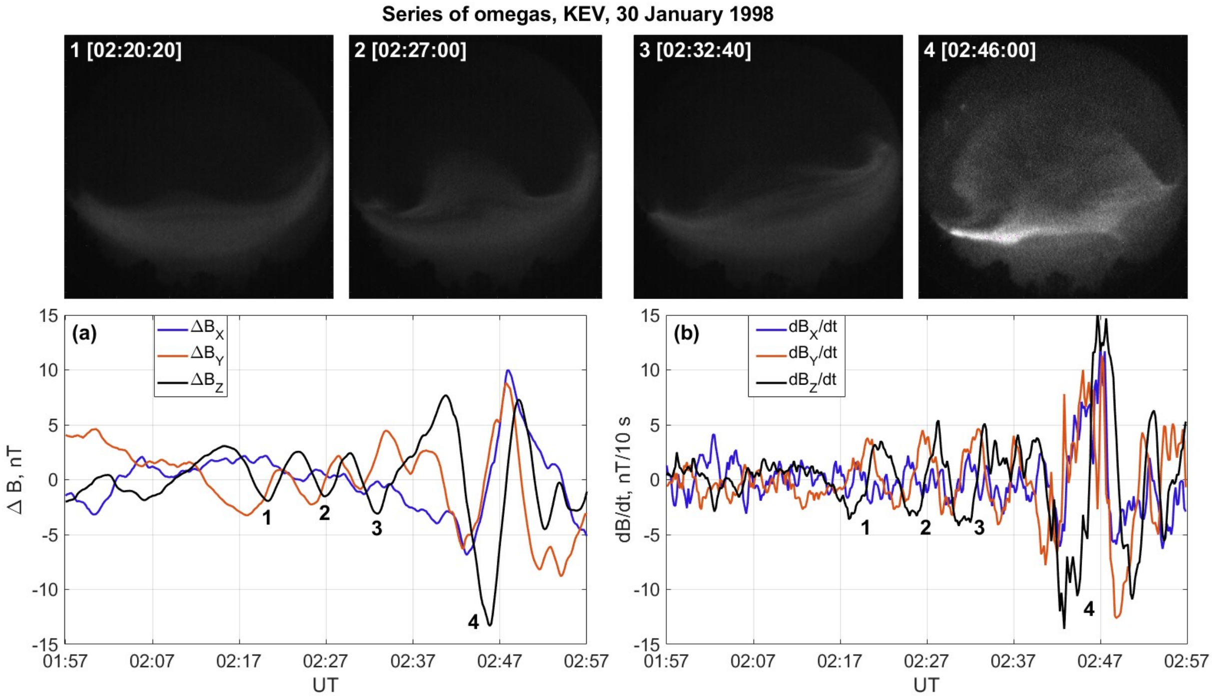

Figure 4. (a) Variations in the northward X (blue), eastward Y (red), and downward Z (black) geomagnetic field components at the Kevo station from 02 to 03 UT, 30 January 1998. The numbers in ASC images at the upper left corner correspond to the variations indicated with numbers 1-4; omega #2 is from the list by Partamies et al. 2017. (b) time derivatives of the magnetic field components.

An example of magnetic field variations at Kevo station on 30 January 1998 is shown in Figure 4. This example from the analyzed list nicely corresponds to the signature revealed in Figure 3a. P17 includes only one omega at 02:27 UT (omega #2 in Figure 4), while there are certainly more omega signatures within ±30 min interval. Four omega patterns are enumerated below the local minima of Z component (black curve). The ASC images shown on the top panel of Figure 4 confirm that each of these minima indeed corresponds to the auroral omega structure. During this event, the train of the observed omegas produces the quasi-periodic pulsations with 5-10 min period, resembling the known Ps6 type of pulsations observed in Y and Z components of the ground magnetic field in auroral zone and frequently accompanying omega bands (Saito, 1978; Gustafsson et al. 1981; Viljanen et al., 2001).

The amplitude of the magnetic effect from omegas 1-3 is about 50 nT for both Bx and By - twice the amplitude of the superposed epoch result. These omegas occur within 20 minutes - about 7 minutes for each omega. Figure 4b shows that the corresponding time derivatives are about 5 nT/10 s. The biggest and brightest 4-th omega causes the largest variations. Magnetic perturbation of about 150 nT corresponds to very high derivatives of about 10-15 nT/10 s in all magnetic components. The dependence of magnetic derivatives from the area covered by omega is investigated in Section 6.

3.2. Superposed geomagnetic variations

Omega structures may induce significant ground magnetic perturbations up to hundreds of nanoteslas. In the omega band event on 29 June 2013 studied by Apatenkov et al. (2020), time derivatives peaked at 15 nT/s (150 nT/10 s), which led to extremely high GIC in the power grid >100 A. The omega structures in that event were relatively big 120-150·103 km^2, as estimated from DMSP satellite UV images, and fast 0.5-1.7 km/s. Yet it is interesting to estimate the derivatives of the ground magnetic field caused by more regular omegas from the P17 list.

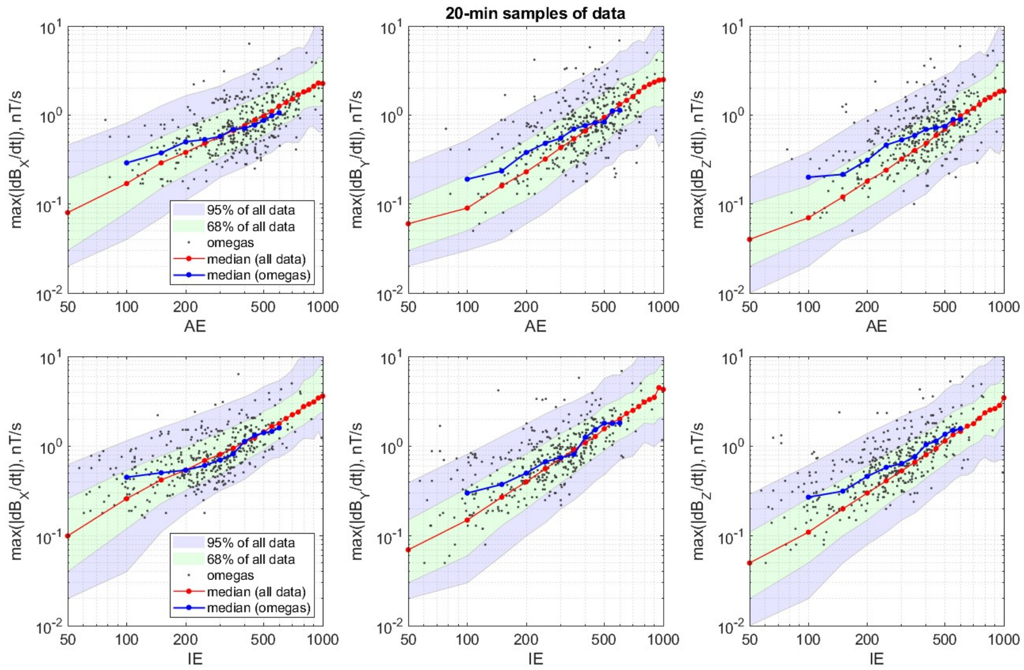

Figure 5. Comparison of the omegas' magnetic field derivatives (scatterplot and blue curve) with all derivatives in this sector (shaded areas and red curve) depending on AE (upper row) and IE (bottom row) activity indices. Blue curve indicates median values for the omegas max|dB/dt| within the ±50 nT window of the corresponding activity index. Shaded areas characterize distribution of maximum |dB/dt| values for all 20-min samples of the corresponding magnetic data depending on AE/IE indices. Red curve shows the median and shaded blue and green areas show 2.5-97.5% and 16-84% quantiles for all observed values of max|dB/dt| in this sector.

In Figure 5, we show maximum |dB/dt| values (black dots) calculated from the 10-s magnetic observations within ±10 minutes of the average time when omega was seen at the ASC. The derivatives are placed against two geomagnetic indices (averaged within the analyzed 20 min samples) measuring the auroral disturbance: (1) global auroral electrojet AE index (Davis and Sugiura, 1966) which is calculated from the perturbations of H component at auroral observatories covering most of longitude sectors, and (2) local IE electrojet indicator (Partamies et al., 2015) which is calculated in the same way but for IMAGE magnetometer network only. Blue curves indicate median values of maximum |dB/dt| in the ±50nT moving window. Clearly, higher |dB/dt| in all three components of the geomagnetic field correspond to distrubed periods, i.e. to higher AE and IE indices (note the logarithmic scale of both horizontal and vertical axes).

The effect of the omegas on the ground dB/dt can be estimated by comparing with the distribution of maximum |dB/dt| values in arbitrary 20-min samples from IMAGE network selected for the similar to omega conditions. For this, we restrict the time to 1997-2006 and magnetic local time to 01-05 MLT, i.e. corresponding to the time when the analyzed omegas from the P17 list were observed. In Figure 5, the distribution of maximum |dB/dt| values in arbitrary 20-min samples are characterized by the median value, calculated in ±50 nT moving window (red curve), and four quantile levels, indicating 2.5, 16, 84, and 97.5 % of all data within the window. Area between 2.5 and 97.5% is shaded blue. Area between 16 and 84% often related to ± one standard deviation for the normal distribution is shaded green.

Figure 5 reveals that for the same activity level, drifting omega structures produce faster changes in the ground magnetic field, specifically in the Y and Z components. Higher |dB/dt| derivatives for omegas, as compared to baseline values obtained within 20-min samples, are more often observed during low and moderate geomagnetic activity below 250(200) nT for AE(IE) for Bx component, below 400(300) nT for By component, and below 500(600) nT for Bz component. Median values of the maximum |dB/dt| for these ranges of AE and IE indices are on average 0.1-0.2 nT/s higher, which is 50-100% higher than the baseline derivatives. Therefore, even regular omegas of small size (fit in the ASC field of view) on average lead to faster changes of the ground geomagnetic field.

3.3. Omega motion

The drift of the omega bands can be investigated from the auroral observations. The all-sky cameras have 20 second cadence, so the majority of omegas from the P17 list were observed at several sequential frames during 1-15 minutes. To track the omega motion, we select three specific points connected to the omega shape, namely (A) western bottom, (B) top point and (C) eastern bottom (Figure 6a). We admit this is subjective, however, the formal method has not been invented yet to our knowledge.

We also note the raw ASC images were mapped to the ionosphere assuming constant 118 km altitude. Near horizon pixels, 70-90 degrees from zenith, were removed as they bear large uncertainties. The mapping procedure described in Syrjasuo (1996) transforms auroral ASC images into rectangular coordinates.

An example of point selection for omega tracking is shown in Figure 6a by blue, green, and purple circles corresponding to the previously described A, B, and C points. We assume the constant velocity for each point, allowing the velocities V_A, V_B, V_C to be different. The time sequence of point locations X(t) is fitted by linear function. This is done independently for X, northward, and Y, eastward, coordinates. So, we find V_X and X_0 in the set of equations $X(t_i) = V_X t_i + X_0$. The same is done for V_Y and Y_0.

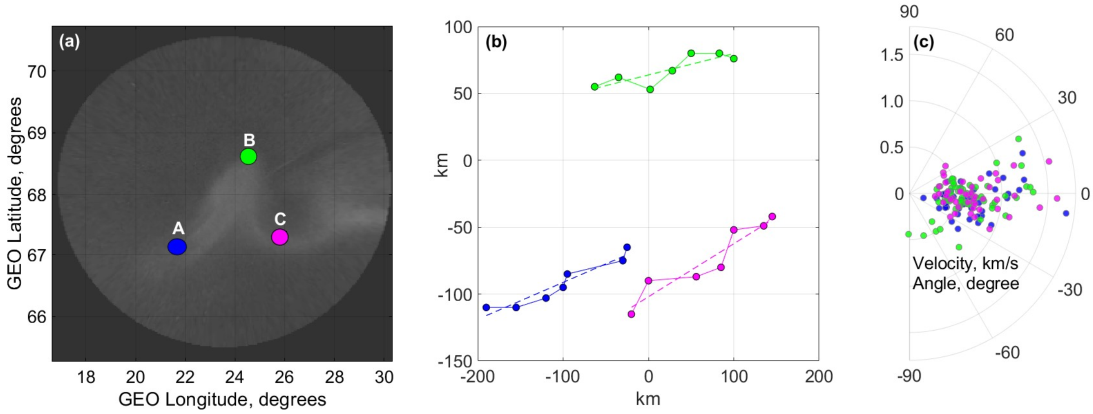

Figure 6. (a) Example of ASC image taken at Muonio on 11 January 2002 at 01:26 UT and three reference points for the analysis of omega velocity and area. (b) linear fit of the coordinates of

each point corresponding to consecutive images of this omega. (c) polar plot for the angles and velocities obtained for the omegas observed at Muonio. Zero direction is the geomagnetic East.

The fitting results are shown in Figure 6b. The dashed lines correspond to the coordinates obtained from the constant velocity approach. The velocities for points A, B, and C in this case slightly differ from each other. $V_A = (V_{AX},V_{AY}) = (0.18, 0.68)$, $V_B = (0.10, 0.72)$, $V_C = (0.31, 0.73)$ km/s. To simplify reading and analysis, we further present velocity absolute value and its direction as the angle (in degrees) with respect to the geomagnetic East (positive is counterclockwise). The difference between geomagnetic and geographic East is about 11 degrees. The (V_{AX},V_{AY}) values from example above transform to (|V|, angle) values, giving $V_A = (0.70, 3.5)$, $V_B = (0.73, -3.5)$, $V_C = (0.79, 11.8)$.

In total we managed to track 433 omega structures based on the P17 list (60 for ABK, 77 for KEV, 105 for KIL, 61 for MUO, and 130 for SOD). The resulting velocities and angles are summarized in Figure 6c for Muonio station and Figure 7 for all five sights. Figure 6c and Figure 7(a,b) demonstrate that the speeds are in the 0.2-2 km/s range, the majority of the directions are within the -30 to +30 degrees sector from the geomagnetic East, the main direction is definitely eastward. The most probable speed values are in 0.2-0.8 km/s range that is in good agreement with previous case studies papers (e.g. Opgenoorth et al., 1983). We did not observe any significant difference between the distributions at any particular station; indeed, all ASC are at a very narrow range of the magnetic latitudes.

There is a visual tendency that the omega velocity distribution is shifted slightly equatorward. The histograms of angle and speed distributions are presented in Figure 7a-b. The equatorward motion tendency is confirmed in Figure 7b, there are more omegas moving slightly equatorward (negative values of the angle) than poleward in addition to main eastward propagation. This equatorward drift can be related either to (1) earthward motion of the magnetospheric source or (2) to the overall expansion of the polar cap and the auroral oval during the substorm development. It is worth noting that if the first statement is correct, then this subtle north-south shift in the distribution of ionospheric velocities can lead to a significant radial velocity of the magnetospheric source. Indeed, in a recent study by Andreeva et al. (2021), the same set of omega cases was magnetically mapped to the equatorial magnetosphere. They showed that the magnetospheric counterpart statistically has the radial velocity component of several tens of km/s, which is comparable to the velocity in the azimuthal direction.

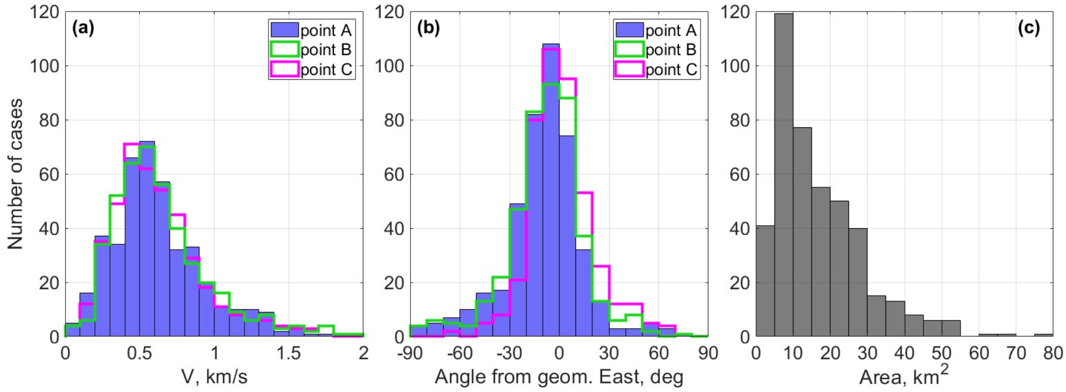

Figure 7. Distributions of omegas velocity (a), angle from geomagnetic East (b), and area (c).

In addition to velocity, we provide rough estimation of the area covered by an omega shown in Figure 7c. We use triangles constructed from the points A, B and C (Figure 6a) to calculate this area. The average area during the omega passage is further considered. The area has values in the range 2-80·103 km^2 with the mean value 18·103 km^2. Note, the upper limit for the omegas' area is instrumentally limited by the size of the ASC field of view in our study. The much larger omegas have been observed by spaceborne imagers. For example, we estimate the omega area from DMSP/SSUSI observations describes by Apatenkov et al. (2020) as 120-150·103 km^2.

3.4. Dependence on omega velocity and area

In order to analyse how time derivatives of the ground magnetic field depend on omega velocity, we consider 433 cases with tracked omegas. As a very rough assumption, we can estimate the relation between ground magnetic field and velocity and area of omegas by considering a linear X-directed equivalent current J_X moving in Y direction above the station. This current may be roughly interpreted as a poleward directed Hall current between two vortices of equivalent currents, associated with each individual omega. Time variation of the magnetic field B in a fixed point on the ground induced by a moving horizontal wire with current J_X (directed strictly northward) in the ionosphere is given by the expression following Biot-Savart law:

$$B(t) = \frac{\mu_0 J_X}{2\pi\sqrt{(H^2+V^2t^2)}}, \qquad \text{(Eq 1)}$$

where H - altitude of the equivalent currents (110 km), V - velocity of the current moving in Y direction, t - time from the omega peak (when the current is right above the station). In assumption of constant J_X and V, we obtain the time derivative for $B(t)$:

$$\frac{dB}{dt} = \frac{\mu_0 J_X V^2 t}{2\pi\sqrt{(H^2+V^2t^2)^3}}, \qquad \text{(Eq 2)}$$

In order to get an expression for the maximum time derivative of the induced magnetic field, we find the root of the equation *(dB/dt)'=0* and substitute it to the Eq 2:

$$\left(\frac{dB}{dt}\right) = \frac{\mu_0 J_X V}{3\pi\sqrt{3}H^2}, \qquad \text{(Eq 3)}$$

Equation 3 indicates the linear dependence of maximum dB/dt on the omegas' velocity. Figures 8(a,d,g,k) show maximum values of time derivatives in 20 min intervals in X (a), Y (d), Z (g) components of the geomagnetic field and its magnitude (k) versus the omegas' velocity (first column). Despite the large spread the tendency for higher dB/dt occurrence during higher velocities is clearly seen, especially in the median values (red circles) for the corresponding ranges of V. Dependence is roughly linear, as predicted by Equation 3.

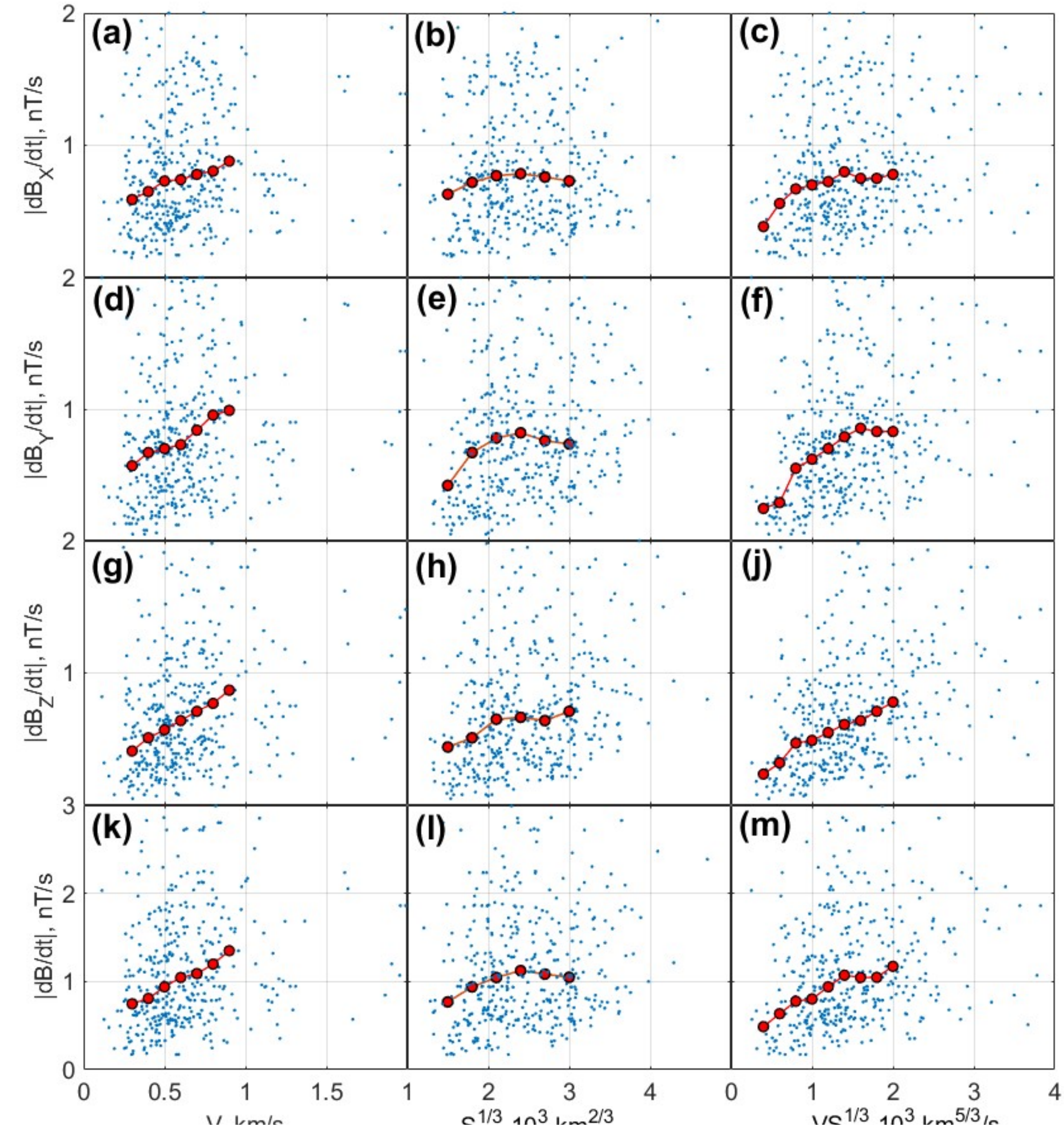

Figure 8. Maximum values of |dB/dt| in X (a-c), Y (d-f), and Z (g-j) geomagnetic field components and their magnitudes (k-m) depending on the omegas' velocity (first column), area $S^{1/3}$ (second column), and $VS^{1/3}$ (third column). Red circles denote median values for the corresponding ranges of V, S, and $VS^{1/3}$.

Here, we also investigate how dB/dt may depend on the area covered by the bright part of the omega (second column, Figure 8(b,e,h,l)). The logic behind it is that larger structures may be associated with stronger currents. Although this relation is weaker than for velocity, we still can see an increase in median dB/dt values. We also found that the relation is better between dB/dt and a product of velocity and area, where area is in the 1/3 degree (third column, Figure 8(c,f,j,m)). These figures indicate that faster and larger omegas provide higher time derivatives of the surface magnetic field.

4 Discussion

In the previous sections, we show that omegas from the P17 list are sources of increased time derivatives of the ground magnetic field (Figure 5). The analyzed omegas are restricted in size by a 2.8105 km^2 circle area covered by the ASC field of view at 118 km altitude. For the P17 list, the largest area of a triangle formed by A, B, and C points is about 0.8105 km^2, one third of the camera's field of view. Larger omegas cannot be tracked using ASCs. Besides, P17 list is a small fraction of the variety of omegas and lacks a representative set of extreme cases (big/fast/faint omegas).

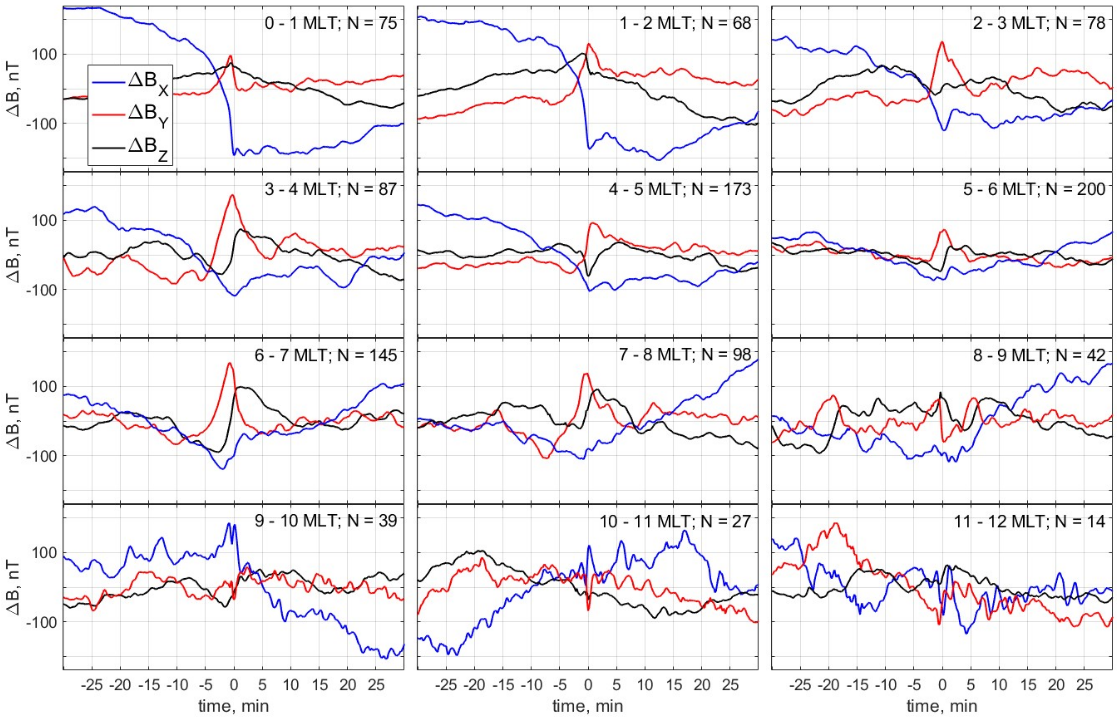

Figure 9. Superposed magnetic variations observed on five Fennoscandia stations with zero time for the cases with |dB/dt|>10nT/s. Number of cases and MLT sectors are shown in each panel.

Apatenkov et al. (2020) show that large scale omega bands can be responsible for extremely high dB/dt values up to 15 nT/s. Using the same 10s magnetic data of five stations during 1996-2018, we search for the time when |dB/dt| was greater than 10 nT/s.

In order to find unique cases, we select only those that are separated by at least one hour. This gives over 1715 cases for five stations (1046 in 00-12 MLT and 669 in 12-24 MLT). In Figure 9, the corresponding variations were superposed like in Section 3 with zero time being the time of maximum |dB/dt|. The results are shown separately for each hour within the 00-12 MLT sector. The interesting finding is that the omega-like magnetic signatures (Section 3, Figure 3a) are clearly observed in the 03-08 MLT sector: negative to positive By change near zero epoch time and the same change in Bz several minutes after.

Note also, that this MLT sector is characterized by the largest number of cases with |dB/dt|>10 nT/s. This is similar to the Ps6 pulsation occurrence distribution (Rostoker and

Barichello, 1980) with maximum in 04-06 MLT. Thus, we speculate that a significant part of the extreme ground dB/dt events at auroral latitudes might be associated with the passage of the omega bands, in agreement with Apatenkov et al. (2004).

5 Conclusions

In this study, we estimate the ground magnetic effect produced by the omega auroral structures. The list provided by Partamies et al 2017 includes 438 omegas observed by the ASCs at the Fennoscandia region. The omegas from this list are highly versatile in form, size (limited by the ASC field of view), velocity, and brightness.

Typical magnetic signature of the ground magnetic perturbation due to omegas was estimated using superposed epoch analysis. We found that the typical magnetic variation has a short time signature: depression of the Z and bipolar variation of the Y geomagnetic field components within ±5 minutes of the omega peak time (when the omega is above the site of the magnetic observations). This reflects the eastward propagation of the WEJ mesoscale bend which has almost north-south directed segments. The variations at the longer time scale, from 30 to 0 minutes before omega peak time, probably denote equatorward expansion of the WEJ which is seen in gradual decrease of X and increase of Z geomagnetic field components. This kind of WEJ behavior usually indicates the global convection growth or substorm expansion.

The moving current system associated with omega causes high dB/dt at the Earth's surface. We found that on average the appearance of omega structures increases the rate of change in the surface magnetic field by 50 to 100% for moderate geomagnetic activity level, as compared to all dB/dt in the morning sector.

We also track omega bands using three reference points manually selected on the ASC images and obtain their average velocities, directions and areas. The velocity range is 0.2-2 km/s with the average value of 0.7 km/s. The directions range from -30 to +30 degrees from the geomagnetic East with the average value of -6 degrees (to the South) indicating small equatorward motion.

Linear dependence was found between dB/dt and omega velocity, verifying that faster omegas induce higher dB/dt on the ground. Although the omega size seems to have a weaker effect on dB/dt, the product of the velocity and area shows better correlation than with only velocity.

Moreover, it was found that the highest dB/dt values observed at the Fennoscandia region in 1996-2018 within 03-08 MLT sector ressemble the omega magnetic signatures. Extremely big/intense/fast omega bands therefore might be responsible for the fast changes of the ground magnetic field and thus triggering the formation of intense GIC.

Acknowledgments

We thank the institutes who maintain the IMAGE Magnetometer Array: Tromsø Geophysical Observatory of UiT the Arctic University of Norway (Norway), Finnish Meteorological Institute (Finland), Institute of Geophysics Polish Academy of Sciences (Poland), GFZ German Research Centre for Geosciences (Germany), Geological Survey of Sweden (Sweden), Swedish Institute of Space Physics (Sweden), Sodankylä Geophysical Observatory of the University of Oulu (Finland), and Polar Geophysical Institute (Russia).

The MIRACLE data could be requested at https://space.fmi.fi/MIRACLE/. The list of omega events from Partamies et al. (2017) is available at http://doi.org/10.5281/zenodo.4541669.

The work by M.V., V.A., S.A. and E.G. was supported by Russian Science Foundation grant 19-77-10016.

The work of L.J. and K.K. was supported by the Academy of Finland (decision 314670).

The visits of V.A., S.A., and E.G. to FMI were supported by the Academy of Finland fund: Space Cooperation in the Science and Technology Commission between Finland and Russia (TT/AVA).

References

Akasofu, S.I. (1974). A study of auroral displays photographed from the DMSP-2 satellite and from the Alaska meridian chain of stations. Space Sci Rev 16, 617–725. https://doi.org/10.1007/BF00182598

Akasofu, S. I. and Kimball, D. S. (1964). The dynamics of the aurora-1. Instabilities of the aurora, J. Atmos. Terr. Phys., 26, 205–211. https://doi.org/10.1016/0021-9169(64)90147-3.

Amm, O., Aksnes, A., Stadsnes, J., stgaard, R., N.and Vondrak, Germany, G., Lu, G., & Viljanen, A. (2005). Mesoscale ionospheric electrodynamics of omega bands determined from ground-based electromagnetic and satellite optical observations. Ann.Geophys, 23 , 325-342.

Apatenkov, S.V., Sergeev, V.A., Pirjola, R., Viljanen, A., (2004). Evaluation of the geometry of ionospheric current systems related to rapid geomagnetic variations. Ann. Geophys. 22, 63–72.

Apatenkov, S. V., Pilipenko, V. A., Gordeev, E. I., Viljanen, A., Juusola, L., Belakhovsky, V. B., Sakharov Ya.A., Selivanov, V. N. (2020). Auroral omega bands are a significant cause of large geomagnetically induced currents. Geophysical Research Letters, 47, e2019GL086677. https://doi.org/10.1029/2019GL086677

Cagniard, L. (1953) Basic Theory of the Magneto-Telluric Method of Geophysical Prospecting. Geophysics, 18, 605-635, https://doi.org/10.1190/1.1437915

Davis, T. N., and Sugiura, M. (1966), Auroral electrojet activity index AE and its universal time variations, J. Geophys. Res., 71(3), 785– 801, doi:10.1029/JZ071i003p00785.

Gustafsson, G., Baumjohann, W., & Iversen, I. (1981). Multi-method observations and modelling of the three-dimensional currents associated with a very strong Ps6 event. Journal of Geophysics, 49 , 138-145.

Henderson, M. G., Kepko, L., Spence, H., Connors, M., Sigwarth, J., Frank, L., et al. (2001). The evolution of north-south aligned auroral forms into auroral torch structures: The generation of omega bands and ps6 pulsations via flow bursts. Proc. Sixth Int. Conf. on Substorms, 169-174.

Heyns, M. J., Lotz, S. I., & Gaunt, C. T. (2021). Geomagnetic pulsations driving geomagnetically induced currents. Space Weather, 19, e2020SW002557. https://doi.org/10.1029/2020SW002557D.

Jorgensen, A. M., Spence, H. E., Hughes, T. J., and McDiarmid, D. (1999). A study of omega bands and Ps6 pulsations on the ground, at low altitude and at geostationary orbit, J. Geophys. Res., 104(A7), 14705– 14715, doi:10.1029/1998JA900100.

Liu, J., Lyons, L. R., Archer, W. E., Gallardo-Lacourt, B., Nishimura, Y., Zou, Y., Gabrielse, C., Weygand, J. M. (2018). Flow shears at the poleward boundary of omega bands observed during conjunctions of Swarm and THEMIS ASI. Geophysical Research Letters, 45, 1218-1227, https://doi.org/10.1002/2017GL076485.

Oyedokun, M. Heyns, P. Cilliers and C. Gaunt (2020). Frequency Components of Geomagnetically Induced Currents for Power System Modelling, 2020 International SAUPEC/RobMech/PRASA Conference, Cape Town, South Africa, 2020, pp. 1-6, doi: 10.1109/SAUPEC/RobMech/PRASA48453.2020.9041021.

Opgenoorth, H. J., Oksman, J., Kaila, K. U., Nielsen, E., and Baumjohann, W. (1983). Characteristics of eastward drifting omega bands in the morning sector of the auroral oval, J. Geophys. Res., 88, 9171.

Opgenoorth, H.J.,Persson,M.A.L.,Pulkkinen,T.I.,Pellinen,R.J. (1994). Recovery phase of magnetospheric substorms and its association with morning sector aurora. J. Geophys. Res. 99, 4115–4129. http://dx.doi.org/10.1029/93JA01502.

Partamies, N., Juusola, L., Whiter, D., and Kauristie, K. (2015). Substorm evolution of auroral structures, J. Geophys. Res. Space Physics, 120, 5958– 5972, doi:10.1002/2015JA021217.

Partamies, N., Weygand, J. M., & Juusola, L. (2017). Statistical study of auroral omega bands. Annales Geophysicae, 35 , 1069-1083. doi: 10.5194/angeo-35 -1069-2017

Pulkkinen, A., et al. (2017). Geomagnetically induced currents: Science, engineering, and applications readiness, Space Weather, 15, 828–856, doi:10.1002/2016SW001501.

Rostoker, G., and Barichello, J. C. (1980). Seasonal and diurnal variation of Ps 6 magnetic disturbances, J. Geophys. Res., 85(A1), 161– 163, doi:10.1029/JA085iA01p00161.

Saito, T. (1978). Long-period irregular magnetic pulsation, Pi3. Space Sci Rev 21, 427–467. https://doi.org/10.1007/BF00173068.

Sergeev, V. A., Yahnin, D. A., Liou, K., Thomsen, M. F., & Reeves, G. D. (2003). Narrow plasma streams as a candidate to populate the inner magnetosphere. In T. I. Pulkkinen, N. A. Tsyganenko, & R. H.W. Friedel (Eds.), The inner magnetosphere, Geophysical Monograph Series (pp. 55–60). United States: American Geophysical Union. https://doi.org/10.1029/155GM07

Syrjäsuo, M. (1996). All-sky camera, Master's thesis, Helsinki University of Technology.

Tanaka, Y., Ogawa, Y., Kadokura, A. et al. (2015). Eastward-expanding auroral surges observed in the post-midnight sector during a multiple-onset substorm. Earth Planet Sp 67, 182. https://doi.org/10.1186/s40623-015-0350-8

Tanskanen, E.I. (2009): A comprehensive high-throughput analysis of substorms observed by IMAGE magnetometer network: Years 1993-2003 examined. J. Geophys. Res., 114, A05204, doi:10.1029/2008JA013682

Tsyganenko, N. A., & Andreeva, V. A. (2016). An empirical rbf model of 601 the magnetosphere parameterized by interplanetary and ground-based 602 drivers. J. Geophys. Res. Space Physics, 121 (11), 10,786-10,802. doi:603 10.1002/2016JA023217

Viljanen, A., Nevanlinna, H., Pajunpää, K., & Pulkkinen, A. (2001). Time derivative of the horizontal geomagnetic field as an activity indicator. Annales Geophysicae, 19(9), 1107–1118. https://doi.org/10.5194/angeo-19-1107-2001

J.M. Weygand, M.G. Kivelson, H.U. Frey, J.V. Rodriguez, V. Angelopoulos, R. Redmon, J. Barker-Ream, A. Grocott, O. Amm (2015). An interpretation of spacecraft and ground based observations of multiple omega band events. Journal of Atmospheric and Solar-Terrestrial Physics, 133 , 185-204. https://doi.org/10.1016/j.jastp.2015.08.014

Wild, J. A., Woodfield, E. E., Donovan, E., Fear, R. C., Grocott, A., Lester, M., Fazakerley, A. N., Lucek, E., Khotyaintsev, Y., Andre, M., Kadokura, A., Hosokawa, K., Carlson, C., McFadden, J. P., Glassmeier, K. H., Angelopoulos, V., and Björnsson, G. (2011). Midnight sector observations of auroral omega bands, J. Geophys. Res., 116, A00I30, https://doi.org/10.1029/2010JA015874.